Materials Horizons

ROYAL SOCIETY OF CHEMISTRY

COMMUNICATION

View Article Online
View Journal | View Issue

Cite this: *Mater. Horiz.*, 2022, 9, 748

Received 23rd June 2021,
Accepted 23rd November 2021

DOI: 10.1039/d1mh00975c

rsc.li/materials-horizons

The discovery of a superhard P-type transparent semiconductor: $Al_{2.69}B_{50}$†

Xu Zheng, ‡[ab] Dayu Yan,‡[a] Changjiang Yi,‡[a] Jinlong Zhu,[c] Qinghua Zhang,[a] Junyi Zhai,[d] Teng Ma,[e] Pinwen Zhu,[e] Hui Li,[a] Lin Gu,[af] Yusheng Zhao,[c] Yugui Yao,[b] Youguo Shi,*[a] Xiaohui Yu*[a] and Changqing Jin*[a]

Superhard semiconductors have been long sought after for electronic device applications enduring extreme conditions, such as astronautics, due to their intrinsic toughness, high thermal and chemical stability. Here, we report the superhard p-type semiconductor $Al_{2.69}B_{50}$ single crystal with the determined Vickers hardness of ~40.5 GPa under the load of 0.49 N, which is one of the hardest semiconductor compounds that have been ever found. With the direct band gap of 2.3 eV, $Al_{2.69}B_{50}$ exhibits excellent optical transmittance (>90%), covering the visible range from 459 nm to 760 nm and part of the infrared range, and also shows the high intensity of the photon emission in the visible light. $Al_{2.69}B_{50}$ is very stable, thermally and chemically, with an ultra-low density of ~2.52 g cm^{-3}, allowing for further extension of its applications. Such an assembly of various excellent properties within one material has great implication for high power electronic design and applications.

New concepts

In this work, we present the design and synthesis of a new functional material, $Al_{2.69}B_{50}$ single crystal with complex boron frameworks, which is a very important discovery as there are very few new binary compounds waiting to be discovered. The $Al_{2.69}B_{50}$ single crystal possesses high mechanical strength with the determined Vickers hardness of ~40.5 GPa under the load of 0.49 N, indicating its superhard property. Under a 10 μm thickness, the resulting materials displays excellent optical transmittance at ~100%, which covers the visible range from 459 nm to 760 nm and part of the infrared range. It also shows the high intensity of the photon emission in the visible light. $Al_{2.69}B_{50}$ is a direct band p-type semiconductor with a band gap of about 2.3 eV, and shows high electronic conductivity (0.011 S m^{-1}) at room temperature. Additionally, $Al_{2.69}B_{50}$ is very stable thermally and chemically, with an ultra-low density of ~2.52 g cm^{-3}, which can further extend its applications. Hence, $Al_{2.69}B_{50}$ is a multifunctional material showing various excellent properties, which has great implication to the development of highly efficient electronic devices and promotion of relevant applications.

Introduction

The synthesis of functional materials that possess excellent electrical, optical and mechanical properties is of fundamental importance to modern industries. The evolution or combination of either of the above properties might revolutionize the modern electrical technology and advance the basic theory of material sciences.[1–3] For example, applications of information technology, light emitting devices (LEDs) and solar cells have benefited substantially from the development of transparent and conductive semiconductors, such as III–V nitrides and transition metal oxides (*e.g.*, GaN, ZnO).[4–6] Such a unique combination of optical and electrical properties mainly originates from their special band structures and delicate doping and filming techniques.[7–10] However, because of the large effective mass of holes in oxides/nitrides, most of these semiconductors are intrinsic n-type.[11] Furthermore, due to the poor mechanical strength, the surface of these semiconductors can be easily scratched during polishing, fabricating or even utilizing, leading to significant deterioration of their electrical/optical properties.[12–14] Packaging with plastic, epoxy resin and glass covers may protect the semiconductor devices during operation. However, the mechanical properties of these devices are still barely satisfactory. They may be easily damaged especially in harsh environments, *e.g.*, deep space.[15,16] If the mechanical strength of semiconductor materials can be

[a] *Beijing National Laboratory for Condensed Matter Physics and Institute of Physics, Chinese Academy of Sciences, Beijing 100190, China. E-mail: yuxh@iphy.ac.cn, jin@iphy.ac.cn, ygshi@iphy.ac.cn*
[b] *School of Physics, Beijing Institute of Technology, Beijing 100081, China*
[c] *Department of Physics, South University of Science and Technology of China, Shenzhen 518055, China*
[d] *Beijing Institute of Nanoenergy and Nanosystems, Chinese Academy of Sciences, Beijing 100083, China*
[e] *State Key Laboratory of Superhard Materials, College of Physics, Jilin University, Changchun 130012, China*
[f] *Collaborative Innovation Center of Quantum Matter, Beijing 100190, China*

† Electronic supplementary information (ESI) available. See DOI: 10.1039/d1mh00975c

‡ These authors contributed equally to this work.

enhanced, related wafers will also experience less fragmentation in the chip process and the number of wafers can be increased from the crystal rods.[17] Therefore, it is very important to develop a new generation of superhard p-type semiconductors that can possess intrinsic high toughness.

For the conventional superhard materials, such as diamond, c-BN, and B_6O, the pure and strong covalent bonding network based on B–C–N–O systems is believed to provide both low elastic compressibility (high bulk modulus) and the high resistance to plastic deformation (high hardness). Nevertheless, such pure localized covalence bonds also discourage electron transport, making them large-gap insulators. During the last decade, the transition metal borides have attracted substantial attention because they may simultaneously possess rich electronic properties and high mechanical strength.[18–21] As commonly accepted, the high hardness is attributed to the strong directional covalent bonds within the light element boron network. Meanwhile, doping a transition metal into boron frameworks can modulate the electronic properties (*e.g.*, band gap) with the favorable mechanical strength still preserved. Unfortunately, most transition metal borides with relatively low boron ratio, *e.g.*, ReB_2[19] and CrB,[22] are non-transparent because of their narrow or even metallic band structure. Nevertheless, in the case of very high boron component metal borides,[23,24] it is very promising to find the wide band gap semiconductors with super high hardness because the metal atoms are totally besieged or sandwiched by the boron networks.[25,26]

In this study, we synthesized the $Al_{2.69}B_{50}$ single crystal, which is a p-type semiconductor exhibiting high transparency, substantially high hardness and electronic conductivity (0.011 S m^{-1} at room temperature). More excitingly, the $Al_{2.69}B_{50}$ crystal also possesses low density (2.52 g cm^{-3}), high thermal stability and photoemission in visible light, which are all very important for LEDs.[27,28] Such an assembly of these excellent properties on one material has great implication in the development of high power electronics and may promote relevant applications.

Results and discussion

Crystal structure of the $Al_{2.69}B_{50}$ single crystal

We analyzed the structure based on the diffraction data from a single crystal. Because of the co-existence of a superlattice and twinning, the crystal structure is very complex. In order to reduce the difficulty of solving this structure, only the atomic positions of the subcell are given in this paper, indicating that the actual crystal structure is an intermediate between a superlattice and subcell. $Al_{2.69}B_{50}$ crystallizes in an orthorhombic structure with the *Cmma* space group, which is similar to that of β-AlB_{12} and other reported high boron compounds,[29–38] but with completely different boron atoms. The refined molar ratio of Al : B from the single crystal diffraction data is 2.69 : 50, which is validated by EPMA data (see Table S1, ESI†). The crystal cell parameters (a = 12.661 Å, b = 12.337 Å, c = 5.093 Å) and atom fractional coordinates from the refinement are listed in Table S2 (ESI†). The crystal structure of $Al_{2.69}B_{50}$ has been deposited with the Cambridge Crystallographic Data Centre (CCDC).[39] In the $Al_{2.69}B_{50}$ crystal, the blue AL1/AL1A and AL2 atoms are orthogonally distributed and encapsulated in the yellow B atoms icosahedron clusters formed by $B_{1,2,7,8}$ or $B_{3,4,5,6}$, and these B icosahedron clusters are bridged by B_9 along the a axis, forming a 3D framework (see Table S2 (ESI†) and Fig. 1). We also applied the scanning transmission electron

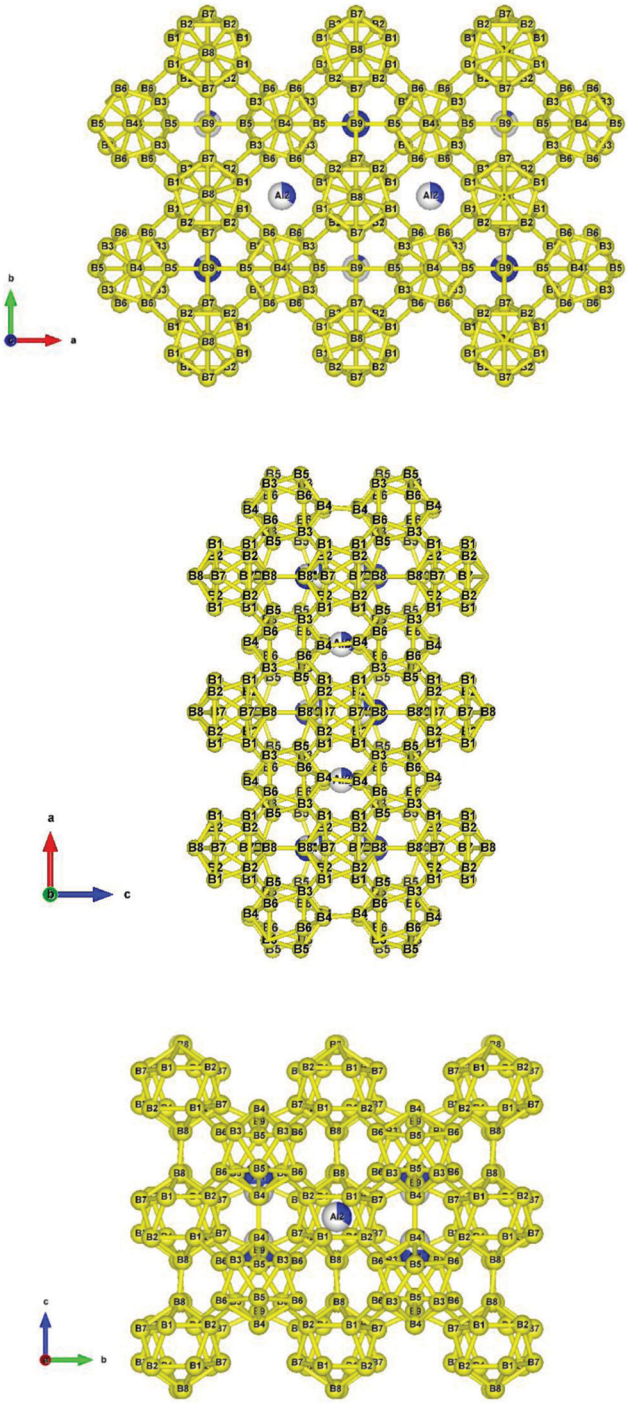

Fig. 1 The crystal structure of the $Al_{2.69}B_{50}$ view along the [001], [100], [010] directions, respectively. The blue balls represent Al atoms and the yellow ones represent B atoms.

microscopy (STEM) annular bright field (ABF) imaging method, and then measured the $Al_{2.69}B_{50}$ single crystal along the [001], [010], [111] projection directions (see Fig. S2, ESI†). According to the STEM images, the inter-planar crystal *d*-spacing can be calculated as $d_{(100)} \approx 6.1$ Å, $d_{(010)} \approx 6.2$ Å, and $d_{(001)} \approx 4.9$ Å, which agree well with the refined unit cell parameters as listed above. The structure refined from single crystal X-ray diffractions along the [001], [010], [111] directions (Fig. 1) is also identical to that of the STEM images.[40,41] The refined average bond length of the B clusters is 1.8 Å, which is almost similar to that of ZrB_{12} (1.78 Å) and B_6O (1.81 Å), indicating the high hardness of $Al_{2.69}B_{50}$. The density of $Al_{2.69}B_{50}$, measured by Archimedes method, is about 2.52 g cm^{-3}, much smaller than that of the most famous superhard materials, WB_4, ZrB_{12} and ReB_2,[18–20] and even lower than that of aluminum. Traditional conductive superhard materials (like WB_4, ZrB_{12} and ReB_2) are compounds composed of transition metal elements and some light elements, such as B, C, and N. In general, the density of these compounds is lower than their simple substance, but because of the relatively high density of the transition metal itself, traditional superhard materials are heavy. The No. 13 element aluminum not only has low density, but also has good metallicity. Due to the high boron content, the density of $Al_{2.69}B_{50}$ is about 2.52 g cm^{-3} ($Density_{[cal]}$ = 2.588 g cm^{-3}), which is much smaller than that of the most famous superhard materials and even lower than that of aluminum.

Mechanical properties of the $Al_{2.69}B_{50}$ single crystal

After polishing the surface of the samples, Vickers hardness (Hv) measurements (under a load of 0.098–9.8 N) were performed on a $Al_{2.69}B_{50}$ single crystal. As shown in Fig. 2, under the load of 0.49 N, the Hv approaches 40.5 GPa, which is comparable to that of some well-known superhard materials, such as ReB_2.[19,21] According to the criterion proposed by Kaner and colleagues,[19,20,42,43] the super-hardness can also be defined under a relatively low load of 0.49 N with Hv $\geq$ 40 GPa. On this basis, $Al_{2.69}B_{50}$ should be another boride with super hardness. On the other hand, when the load is increased from 0.098 to 9.8 N, the measured Hv decreases sharply at first and then saturates around 28 GPa, suggesting that $Al_{2.69}B_{50}$ is intrinsically in the regime of hard materials. Nevertheless, as is shown from Fig. 2 and Fig. S3 (ESI†), this hardness value is still much higher than that of AlN, ZnO, and GaN and other famous semiconductors. Therefore, it could be considered as a potential material for high hardness ultraviolet LEDs and laser diode fields, and used in harsh environments. The fracture toughness of the $Al_{2.69}B_{50}$ single crystal has been characterized and calculated by the following equation:

$$K_{IC} = \xi(E/H_v)^{1/2}(P/c^{3/2})(\text{MPa } m^{1/2})$$

where ξ is the calibration constant of 0.0166 ($\pm$0.004), E is the Young's modulus (GPa) (in the experiment, we used the aggregate Young's modulus, 546.7 GPa, which is measured by nano hardness), P is the loading force (N), and c is the length of the crack. The resulting K_{IC} of the prepared sample occurs at P = 4.9 N and reaches 2.6 MPa $m^{1/2}$, which is equivalent to the value of the single crystal cBN (2.8 MPa $m^{1/2}$).

The phase stability and compressibility of $Al_{2.69}B_{50}$ were investigated by synchrotron X-ray diffraction and Raman spectra in a diamond anvil cell (DAC) with neon as the pressure medium and ruby chip for pressure calibration. The equation of the state (EOS) data of the $Al_{2.69}B_{50}$ powders with pressure up to 40 GPa is shown in Fig. S4 (ESI†). $Al_{2.69}B_{50}$ is structurally stable up to 40 GPa with no phase transition observed (Fig. S5, ESI†). A fit to the Third-order Birch–Murnaghan EOS of the orthorhombic phase gives the bulk modulus B_0 = 243.4(4) GPa. Although the metal element aluminum itself has a low bulk modulus, its building block with a covalent bond connecting small atoms boron has a high bulk modulus close to that of B_6O (222 GPa).[47]

As commonly accepted, the hard/superhard transition metal borides always possess excellent thermal and chemical stabilities because of the strong covalent B–B networks.[48] To investigate the thermal behavior of the $Al_{2.69}B_{50}$ single crystal, thermal gravimetric analysis (TG) and differential scanning calorimetry (DSC) were measured from 0 to 1500 °C (the upper limit of our instrument). As exhibited in Fig. S6 (ESI†), the material was quite stable and kept the initial mass m_0 = 4.3 mg during the entire heating temperature range. The heat flow showed a gradual rising trend with no peak or dip in the testing temperature range, confirming the high thermal stability of $Al_{2.69}B_{50}$. Furthermore, it did not react with most of the alkalis and acids, such as sodium hydroxide and hydrochloric acid, indicating the high chemical stability of this material. Such outstanding thermal and chemical stability is specially demanded in superhard materials and semiconductor industries.

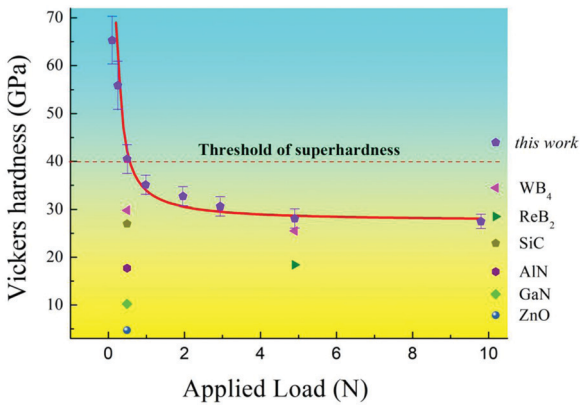

Fig. 2 Mechanical properties of the $Al_{2.69}B_{50}$ single crystal. The Vickers hardness of $Al_{2.69}B_{50}$ is presented as a function of applied loads from 0.098 to 9.8 N. The Vickers hardness of some other famous superhard materials and semiconductors are also compared with $Al_{2.69}B_{50}$.

Transparency and photoluminescence of the $Al_{2.69}B_{50}$ single crystal

It is well known that the band-gap is very important for functional semiconductors, as it influences the transparency,

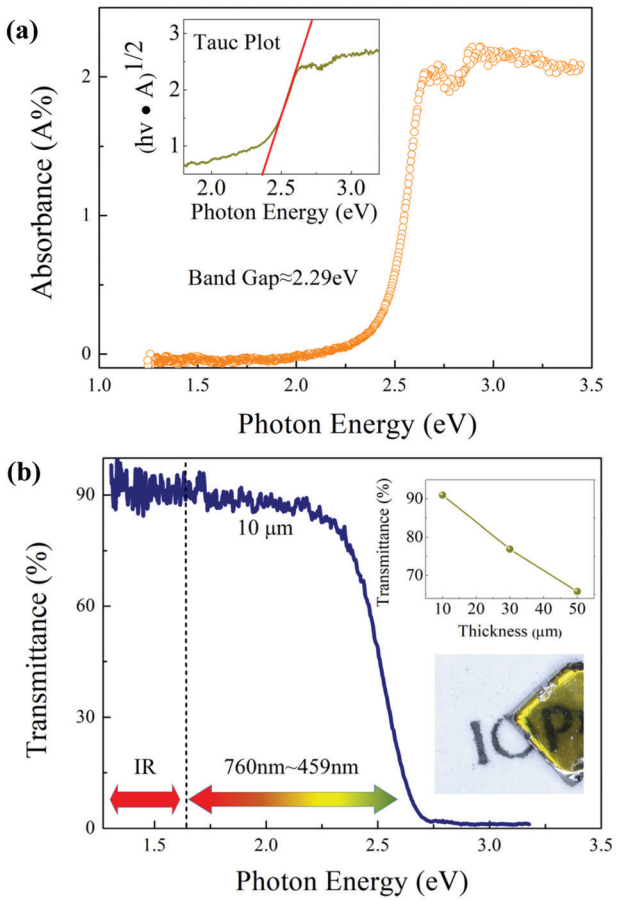

Fig. 3 Optical properties of the $Al_{2.69}B_{50}$ single crystal. (a) Absorbance spectra of the $Al_{2.69}B_{50}$ single crystal by UV-vis measurements at room temperature. The orange circle is the absorbance of $Al_{2.69}B_{50}$ and the insert curve is fitted by Tauc plot $(h\nu \times A)^{1/r}$ with $r = 1/2$. (b) Photon energy dependence of the transmittance of the $Al_{2.69}B_{50}$ single crystal. The insert shows the transmittance increasing as the thicknesses decreases from 50 to 10 μm.

photoluminescence, and electroconductivity.[6–8] The optical band gap of the $Al_{2.69}B_{50}$ single crystal was obtained from the ultraviolet–visible (UV-vis) absorption spectrum fitted by Tauc plot[49,50] with the value of the exponent $r = 1/2$[51,52] (shown in Fig. 3a). A sharp peak indicates that the direct optical band gap is about 2.3 eV, which belongs to the visible range. Moreover, the mechanical and thermal properties mentioned above still have a major impact on the stability and durability of functional materials. In order to show more clearly, some well-known superhard and semiconductors are listed and compared in Table 1. It is shown that the intrinsic band gap (2.3 eV) of $Al_{2.69}B_{50}$ with high hardness offers a tremendous advantage, owing to the excellent optical properties, and has the potential to be one of the most precious and valuable optical detectors.

We further examined the $Al_{2.69}B_{50}$ single crystal in terms of extraordinary light transmittance. As shown in Fig. 3b, it is worth noting that the $Al_{2.69}B_{50}$ single crystal under a 10 μm thickness displays superior transmittance at higher than 90%, and the light transmittance range spans from 459 nm to 1000 nm. In contrast, the transmittance of traditional metal oxide semiconductors (*e.g.*, NiO_x, ZnO) may achieve the same transmittance only with a thickness of the film down to the nanoscale.[55] When the thickness increases from 10 μm to 50 μm perpendicular to the incident light, no notable changes were detected in the absorption edge, while the transmittance of the $Al_{2.69}B_{50}$ single crystal decreased. As shown in the inset of Fig. 3b, there are three letters with the "P" letter clearly visible under the $Al_{2.69}B_{50}$ single crystal with 1 mm × 1 mm × 0.3 mm (thickness), demonstrating excellent transparency even if the thickness approaches the millimeter scale. Therefore, the $Al_{2.69}B_{50}$ single crystal with higher transparency under micrometer scale would show outstanding performance in transparent photovoltaics.

Table 1 The Vickers hardness and bandgap of $Al_{2.69}B_{50}$ compared with some typical famous hard/superhard materials and semiconductors

Materials	Band gap (eV)	Vickers hardness (GPa)
WB_4 (ref. 20)	**Metal**	**29.8[a], 25.5[b]**
ReB_2 (ref. 21)	**Metal**	**18.4[b]**
$Al_{2.69}B_{50}$ (this work)	*2.3*	*40.5[a], 28[b]*
α-SiC (ref. 45)	*2.86*	*27[a]*
ZnO (ref. 45 and 53)	*3.2*	*4.7[a]*
GaN (ref. 45 and 54)	*3.39*	*10.2[a]*
Diamond	***5.5***	***70–100***
AlN (ref. 46 and 54)	***6.2***	***17.7[a]***
c-BN (ref. 44)	***6.4***	***45–50[b]***
α-Al_2O_3 (ref. 45)	***9***	***17.7[a]***

[a] With an applied load of 0.5 N. [b] With an applied load of 4.9 N.The entries in bold represent the metal materials, the entries in italics represent the semiconductor materials, and the entries in bold-italics font represent the insulator materials.

We also conducted photoluminescence (PL) measurements on the $Al_{2.69}B_{50}$ single crystal (Fig. S7, ESI†). The PL spectra displays several broad peaks at ~582 nm, which is near the band-edge emission of $Al_{2.69}B_{50}$, corresponding to the energy of about 2.3 eV. The intense broad peaks range from 534 nm to 850 nm, and the photon emission in this range is generally considered to be induced by defects and band-edge, suggesting that the $Al_{2.69}B_{50}$ signal crystal is photo-emitting in the visible light similar to ZnO or some organic polymers.[56,57] Furthermore, deducted from the spectral data, the $Al_{2.69}B_{50}$ crystal emits light covering most of the visible spectrum range and part of the near infrared light. This wide range could prompt the new design and application for next-generation LEDs, while traditional materials like AlGaInP and InGaN can only cover the narrow part of the spectrum.[58,59]

Electrochemical properties of the $Al_{2.69}B_{50}$ single crystal

In Fig. 4a, the temperature dependence of the electrical conductivity (σ) shows a semiconductor behavior, and the conductivity of the $Al_{2.69}B_{50}$ single crystal is 0.011 S m^{-1} at 300 K, smaller than that of ZnO, a distinguished semiconductor. The σ *vs.* $1/T$ Arrhenius plot in Fig. 4a exhibits two linear regimes from 25 K to 100 K and from 200 K to 300 K. The high-T linear region data were fitted by the thermal activation

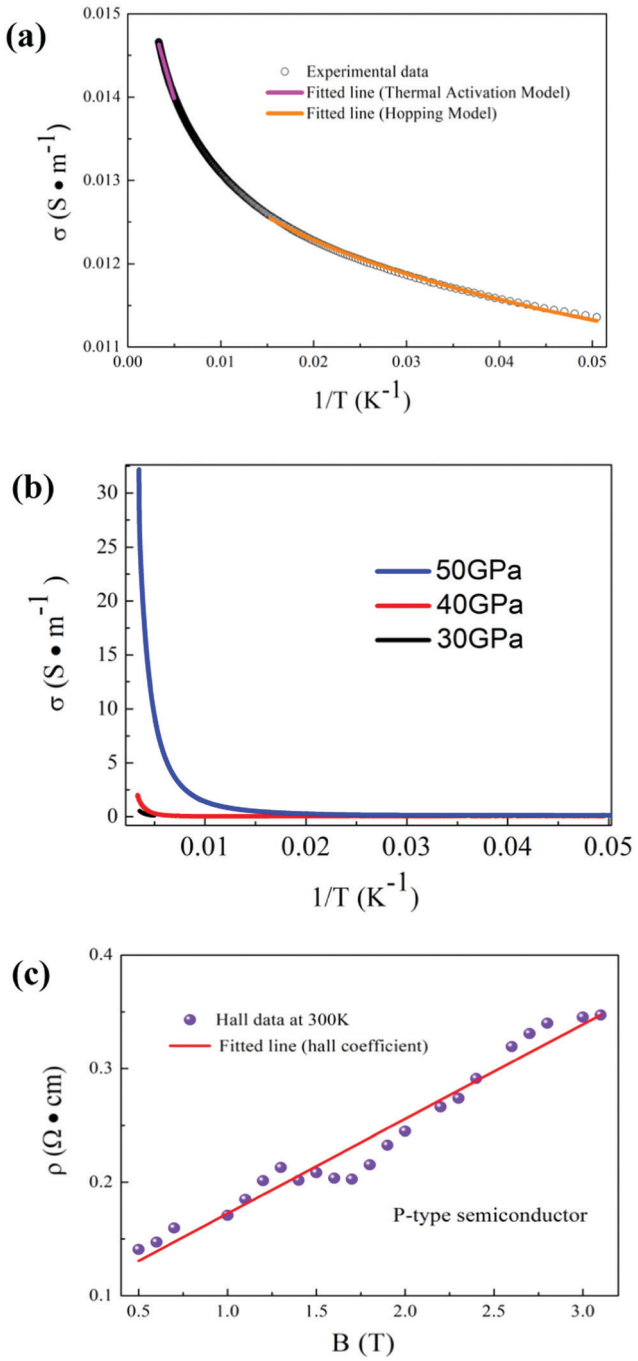

Fig. 4 Electrical properties of the $Al_{2.69}B_{50}$ single crystal. (a) Temperature dependence of the conductivity S of the $Al_{2.69}B_{50}$ single crystal from 300 K to 2 K, indicating its semiconductor behavior. The blue line is fitted by the thermal activation model $\sigma(T) = \sigma_0 \times \exp(-E_a/k_BT)$ in the high T range, and the red line is fitted by the Mott-vrh model $\sigma(T) = \sigma_{vrh} \times \exp[-(T_0/T)^{1/4}]$ in the low T range. (b) Temperature dependence of the conductivity S of the $Al_{2.69}B_{50}$ single crystal from 300 K to 2 K under 30 GPa, 40 GPa and 50 GPa. (c) Hall effect of the $Al_{2.69}B_{50}$ single crystal at 300 K. The slope of the red fitted line is the Hall coefficient (R_H) of $Al_{2.69}B_{50}$. The derived carrier density (n_h), *i.e.*, hole concentration, is 7.5 × 10^{15} cm^{-3}.

model $\sigma(T) = \sigma_0 \times \exp(-E_a/k_BT)$, where σ_0 is the pre-exponential constant, k_B is the Boltzmann constant, and E_a is the activation energy. The low-T linear regime data are well fitted by the hopping model $\sigma(T) = \sigma_{vrh} \times \exp[-(T_0/T)^{1/4}]$, which may be attributed to the variable range hopping (VRH), the saturation regime of the ionization of donors, and very shallow donors.[60] The E_a calculated from the fitting result is 0.0023 eV, *i.e.*, band gap $E_g = 2 \times E_a = 0.0046$ eV. Fig. 4b displays the temperature dependence of the electrical conductivity (σ) at 30 GPa, 40 Gpa and 50 Gpa, respectively. The conductivity of the $Al_{2.69}B_{50}$ single crystal exhibits semiconductor behavior and rises substantially under high pressure. Furthermore, the conductivity of $Al_{2.69}B_{50}$ reaches 32 S m^{-1} at 300 K and 50 Gpa, which shows great semiconductor capability under extreme conditions.

The ρ_{xy}–H curves of the $Al_{2.69}B_{50}$ single crystal at room temperature are shown in Fig. 4c, where the positive Hall coefficient demonstrates the dominant hole type (p-type) carriers. In a single-band model, the hall coefficient R_H is associated with carrier density (n_h) as $R_H = 1/n_he$. Therefore, the fitted hole concentration is 7.5 × 10^{15} cm^{-3}. It is well known that most of the traditional transparent materials,[61,62] *e.g.*, oxides, are n-type semiconductors due to the localization of oxygen, while the $Al_{2.69}B_{50}$ single crystal displays an intrinsic p-type behavior, which may open up a frontier and accelerate the development of functional semiconductors.

Conclusions

In summary, a single crystal $Al_{2.69}B_{50}$ was successfully synthesized and the crystal structure were measured. $Al_{2.69}B_{50}$ possesses high hardness (40.5 GPa under the load of 0.49 N) and bulk modulus (240 GPa). However, unlike the traditional metallic transition metal borides, $Al_{2.69}B_{50}$ exhibits p-type semi-conductivity (direct band gap of 2.3 eV) and unique optical properties. $Al_{2.69}B_{50}$ single crystal possesses high transmittance even under a thickness of 10 μm and photoluminescence in visible light. In addition, it shows high thermal and chemical stability and ultra-low density. Therefore, $Al_{2.69}B_{50}$ demonstrates a set of unique advantages, and can be used as a new multi-functional material applied in substrates, luminous diodes, electron devices and solar cells, and others.

Materials and methods

Synthesis of the $Al_{2.69}B_{50}$ single crystal

Single crystals of $Al_{2.69}B_{50}$ were synthesized by using the Al flux method. High-purity B and Al elements were mixed in a Al_2O_3 crucible with a molar ratio of B : Al = 1 : 10 in a glove box with the protection of high-purity argon. Then, the mixed fine powders were put in a high temperature furnace with argon protection, followed by heating up to 1723 K within 20 hours, and holding at that temperature for additional 2 hours. Then, the furnace was cooled down to 1323 K slowly at a rate of 2 K h^{-1}. After that, the crucibles were reheated to 1173 K to remove the excessive Al flux in a centrifuge. As a result, the $Al_{2.69}B_{50}$ single crystal was obtained.

Vickers hardness measurements

Vickers hardness was measured on the single crystal $Al_{2.69}B_{50}$ with the size of 1 mm × 1 mm× 0.3 mm under various fixed loads of 10 g, 25 g, 50 g, 100 g, 200 g, 300 g, 500 g and 1000 g by using a Micro-hardness tester. All of the measurements were performed with a dwelling time of 15 seconds. Before the measurements, the octahedron-shaped $Al_{2.69}B_{50}$ single crystal was polished on both sides.

High-P synchrotron X-ray diffraction characterization

High-P synchrotron X-ray diffraction experiments were performed by using a diamond-anvil cell (DAC) in the Beijing Synchrotron Radiation Facility (BSRF). The obtained polycrystalline $Al_{2.69}B_{50}$ was grounded into powders and loaded into the sample chamber made of a T_{301} stainless-steel gasket with neon as a pressure-transmitting medium. A few ruby balls were loaded into the same sample chamber to serve as an internal pressure standard. The collected angle-dispersive X-ray diffraction data were analyzed by integrating 2D images as a function of 2θ using the program Fit2D to obtain the conventional, one-dimensional diffraction profiles.

Density measurements

The density of $Al_{2.69}B_{50}$ was measured by Archimedes' method. By choosing an octahedral $Al_{2.69}B_{50}$ single crystal, we denoted the weight as G_0. By tying up the octahedral $Al_{2.69}B_{50}$ single crystal with a hair by a spring balance, we denoted the weight as G_1. Then, we put the $Al_{2.69}B_{50}$ crystal completely in the water, and the weight was denoted as G_2. The density of $Al_{2.69}B_{50}$ was calculated by the formula $\rho = (G_0 \times \rho_{H_2O})/(G_1 - G_2)$.

Transparency measurements

The octahedral $Al_{2.69}B_{50}$ single crystal was polished smoothly by diamond disk, and its properties were characterized by optical microscopy, energy-dispersive X-ray (EDX) analysis, scanning transmission electron microscope (STEM), UV-vis, TG-DSC, and photoluminescence. The photoluminescence experiments were conducted on single crystal $Al_{2.69}B_{50}$ with dimensions of 60 μm × 60 μm × 20 μm by a Renishaw Raman Spectroscopy apparatus equipped with a laser wavelength of 532 nm.

Electrical resistance and carrier concentration measurements

The temperature dependence of resistivity and Hall Effect were measured with the conventional four-probe method in a commercial Physical Property Measurement System (PPMS-9T, Quantum Design). The samples were cut into a rectangular shape with typical dimensions of 0.1 mm × 0.1 mm × 1 mm, for which the longest dimension is along the designed crystallographic direction. Four golden wires with a diameter of 20 μm were attached to the surface of the sample by silver paste, having the excitation current of typical 0.1 mA passing through the outer two probes, while the inner two probes were for voltage signal. The resistivity ρ was calculated from the obtained resistance R through the equation: $\rho = (R \times s)/L$, where s is the cross-section of the sample and L is the distance between the two voltage probes.

Author contributions

Xiaohui Yu and Changqing Jin conceived the project and designed experiments. Xu Zheng, Dayu Yan, Changjiang Yi, Teng Ma, and Youguo Shi carried out most of the experiments. Jinlong Zhu calculated the structure. Qinghua Zhang and Li Gu characterize the structural heterogeneities using Cs-STEM. Xu Zheng, Xiaohui Yu, Junyi Zhai, Pinwen Zhu, Hui Li, Yusheng Zhao, Yugui Yao and Changqing Jin wrote the paper. All authors contributed to the interpretation and presentation of the results.

Conflicts of interest

There are no conflicts to declare.

Acknowledgements

We are grateful to Prof. Carlos-Andres Palma for revisions and improvements. This work was supported by the National Key R&D Program of China (Grants No. 2021YFA1400300, No. 2016YFA0401503, No. 2017YFA0302900, No. 2018YFA0305700, and No. 2016YFA0300604, the China Postdoctoral Science Foundation (2019TQ0039), the National Natural Science Foundation of China (Grants No. 11921004, No.11820101003, No. U2032220, and No. U2032204, the Strategic Priority Research Program and Key Research Program of Frontier Sciences of the Chinese Academy of Sciences (Grants No. XDB33000000, No. XDB25000000, and No. QYZDBSSW-SLH013), the K. C. Wong Education Foundation (No. GJTD-2018-01), the Youth Innovation Promotion Association of Chinese Academy of Sciences (No. 2016006), the Beijing Nature Science Foundation (No. 2202059), the Guangdong Innovative & Entrepreneurial Research Team Program (No. 2016ZT06C279), and the Shenzhen Peacock Plan (No. KQTD2016053019134356). The in situ XRD measurements were performed at 4W2 High Pressure Station, Beijing Synchrotron Radiation Facility (BSRF), which is supported by Chinese Academy of Sciences (Grants No. KJCX2- SWN20 and No. KJCX2-SW-N03). This work was partially carried out at high-pressure synergetic measurement station of Synergic Extreme Condition User Facility.

Notes and references

1 A. D. B. L. Ferreira, P. R. O. Novoa and A. T. Marques, *Compos. Struct.*, 2016, **151**, 3–35.
2 K. Salonitis, J. Pandremenos, J. Paralikas and G. Chryssolouris, *Int. J. Adv. Des. Manuf. Technol.*, 2010, **49**, 803–826.
3 C. Brylinski, *Solid State Phenom.*, 2010, **159**, 19–25.
4 X. Yu, L. Zeng, P. Guo, F. Shi, D. B. Buchholz, Q. Ma, J. Yu, V. P. Dravid, R. P. Chang, T. J. Marks and A. Facchetti, *Adv. Mater.*, 2015, **27**, 2390–2399.

5 T. Sasaki, Y. Endo, M. Nakaya, K. Kanie, A. Nagatomi, K. Tanoue, R. Nakamura and A. Muramatsu, *J. Mater. Chem.*, 2010, **20**, 8153–8157.
6 J. F. Wager, *Science*, 2003, **300**, 1245–1246.
7 H. Kawazoe, H. Yanagi, K. Ueda and H. Hosono, *MRS Bull.*, 2000, **25**, 28–36.
8 H. Moon, H. Cho, M. Kim, K. Takimiya and S. Yoo, *Adv. Mater.*, 2014, **26**, 3105–3110.
9 K. Nomura, H. Ohta, K. Ueda, T. Kamiya, M. Hirano and H. Hosono, *Science*, 2003, **300**, 1269–1272.
10 U. Ozgur, Y. I. Alivov, C. Liu, A. Teke, M. A. Reshchikov, S. Dogan, V. Avrutin, S. J. Cho and H. Morkoc, *J. Appl. Phys.*, 2005, **98**, 041301.
11 G. Hautier, A. Miglio, G. Ceder, G. M. Rignanese and X. Gonze, *Nat. Commun.*, 2013, **4**, 2292.
12 B. L. Sopori, *Rev. Sci. Instrum.*, 1980, **51**, 1513–1515.
13 J. V. Gormley, M. J. Manfra and A. R. Calawa, *Rev. Sci. Instrum.*, 1981, **52**, 1256–1259.
14 R. T. Holm and E. D. Palik, *J. Vac. Sci. Technol.*, 1976, **13**, 889–893.
15 M. Mazur, M. Szymanska, M. Kalisz, D. Kaczmarek and J. Domaradzki, *Surf. Interface Anal.*, 2014, **46**, 827–831.
16 D. Mouricaud, *Optical Systems Design and Production*, 1999, pp. 81–84.
17 G. Coletti, N. J. C. M. Vanderborg, S. DeIuliis, C. J. J. Tool and L. J. Geerligs, Presented at the 21st European Photovoltaic Solar Energy Conference and Exhibition, 2006.
18 T. Ma, H. Li, X. Zheng, S. Wang, X. Wang, H. Zhao, S. Han, J. Liu, P. Zhu, Y. Long, J. Cheng, Y. Ma, Y. Zhao, C. Jin and X. Yu, *Adv. Mater.*, 2017, **29**, 1604003.
19 J. B. Levine, S. L. Nguyen, H. I. Rasool, J. A. Wright, S. E. Brown and R. B. Kaner, *J. Am. Chem. Soc.*, 2008, **130**, 16953–16958.
20 R. Mohammadi, A. T. Lech, M. Xie, B. E. Weaver, M. T. Yeung, S. H. Tolbert and R. B. Kaner, *Proc. Natl. Acad. Sci. U. S. A.*, 2011, **108**, 10958.
21 J. Q. Qin, D. W. He, J. H. Wang, L. M. Fang, Y. L. Li, J. Hu, Z. L. Kou and Y. Bi, *Adv. Mater.*, 2008, **20**, 4780–4783.
22 L. Han, S. M. Wang, J. L. Zhu, S. B. Han, B. J. Chen, X. C. Wang, X. H. Yu, B. C. Liu, R. F. Zhang, Y. W. Long, J. G. Cheng, J. Z. Zhang, Y. S. Zhao and C. Q. Jin, *Appl. Phys. Lett.*, 2015, **106**, 221902.
23 A. Pediadtakis, M. Schroeder, V. Sagawe, T. Ludwig and H. Hillebrecht, *Inorg. Chem.*, 2010, **49**, 10882–10893.
24 H. Duschanek and P. Rogt, *J. Phase Equilib.*, 1994, **15**, 543–544.
25 S. G. Xu, Y. J. Zhao, X. B. Yang and H. Xu, *RSC Adv.*, 2017, **7**, 30320–30326.
26 A. Knappschneider, C. Litterscheid, N. C. George, J. Brgoch, N. Wagner, J. Beck, J. A. Kurzman, R. Seshadri and B. Albert, *Angew. Chem., Int. Ed.*, 2014, **53**, 1684–1688.
27 T. Tamura, T. Setomoto and T. Taguchi, *J. Lumin.*, 2000, **87**, 1180–1182.
28 Y. I. Alivov, U. Ozgur, S. Dogan, C. Liu, Y. Moon, X. Gu, V. Avrutin, Y. Fu and H. Morkoc, *Solid-State Electron.*, 2005, **49**, 1693–1696.
29 S. Okada, K. Kudou and H. Hiyoshi, *et al.*, *J. Ceram. Soc. Jpn.*, 2010, **98**, 1330–1336.
30 H. J. Becher, H. Rethfeld and R. Mattes, *Z. Anorg. Allg. Chem.*, 1975, **414**, 203–210.
31 J. A. Kohn and D. W. Eckart, *Anal. Chem.*, 1960, **32**, 296–298.
32 V. I. Matkovich, J. Economy and R. F. Giese, *J. Am. Chem. Soc.*, 1963, **86**, 2337–2340.
33 H. J. Becher and H. Neidhard, *Acta Crystallogr., Sect. B: Struct. Crystallogr. Cryst. Chem.*, 1968, **24**, 280–281.
34 B. Albert and H. Hillebrecht, *Angew. Chem., Int. Ed.*, 2009, **48**, 8640–8668.
35 A. S. Pediaditakis, M. Schroeder and V. Sagawe, *et al.*, *Inorg. Chem.*, 2010, **49**, 10882–10893.
36 A. A. Berezin, O. A. Golikova and V. K. Zaitsev, *et al.*, *Teubner*, Vieweg, Verlag, 1974.
37 S. E. Colvin, *Teubner*, 1974.
38 A. Grytsiv and P. Rogl, *Aluminium - Boron - Carbon*, Springer, Berlin Heidelberg, 2004.
39 X. Zheng, *Experimental Crystal Structure Determination*, 2021, DOI: 10.5517/ccdc.csd.cc294j66.
40 E. Okunishi, H. Sawada and Y. Kondo, *Micron*, 2012, **43**, 538–544.
41 Y. Wen, T. Shang and G. Lin, *Microscopy*, 2016, **66**, 25–38.
42 H. Y. Chung, M. B. Weinberger, J. B. Levine, A. Kavner, J. M. Yang, S. H. Tolbert and R. B. Kaner, *Science*, 2007, **316**, 436–439.
43 M. T. Yeung, J. Lei, R. Mohammadi, C. L. Turner, Y. Wang, S. H. Tolbert and R. B. Kaner, *Adv. Mater.*, 2016, **28**, 6993–6998.
44 D. W. He, Y. S. Zhao, L. Daemen, J. Qian, T. D. Shen and T. W. Zerda, *Appl. Phys. Lett.*, 2002, **81**, 643.
45 I. Yonenaga, *Phys. B*, 2001, **308–310**, 1150–1152.
46 A. Abid, R. Bensalem and J. Sealy, *J. Mater. Sci.*, 1986, **21**, 1301–1304.
47 S. Lee, D. M. Bylander and L. Kleinman, *Phys. Rev. B: Condens. Matter Mater. Phys.*, 1992, **45**, 3245–3247.
48 N. Kostoglou, K. Polychronopoulou and C. Rebholz, *Vacuum*, 2015, **112**, 42–45.
49 J. Tauc, *Mater. Res. Bull.*, 1968, **2**, 37–46.
50 O. Stenzel, *The Physics of Thin Film Optical Spectra*, Springer Berlin Heidelberg, 2005.
51 J. Tauc, R. Grigorovici and A. Vancu, *Phys. Status Solidi B*, 1966, **15**, 627.
52 E. A. Davis and N. F. Mott, *Philos. Mag.*, 1970, **22**, 903–922.
53 K. H. Lee, C. H. Park, K. Lee, T. Ha, J. H. Kim, J. Yun, G. Lee and S. Im, *Org. Electron.*, 2011, **12**, 1103–1107.
54 B. E. Foutz, S. K. O'Leary, M. S. Shur and L. F. Eastman, *J. Appl. Phys.*, 1999, **85**, 7727.
55 J. M. Choi, D. K. Hwang, J. H. Kim and S. Im, *Appl. Phys. Lett.*, 2005, **86**, 123505.
56 L. Fan, H. Song, T. Li, L. Yu, Z. Liu, G. Pan, Y. Lei, X. Bai, T. Wang, Z. Zheng and X. Kong, *J. Lumin.*, 2007, **122**, 819–821.
57 G. Dobrikov, K. Kolentsov, D. Zhechev, L. Yourukova, M. Rassovska, C. Yossifov and N. Parvanova, *Vacuum*, 2004, **76**, 227–230.

58 A. L. Donne, M. Acciarri, G. Gori, R. Colletto, R. Campesato and S. Binetti, *Sol. Energy Mater. Sol. Cells*, 2010, **94**, 2002–2006.
59 J. H. Rice, R. A. Oliver, J. W. Robinson, J. D. Smith, R. A. Tavlor, G. A. D. Briggs, M. J. Kappers, C. J. Huphrevs and S. Yasin, *Phys. E*, 2004, **21**, 546–550.
60 Z. Xiao, H. Hiramatsu, S. Ueda, Y. Toda, F. Y. Ran, J. Guo, H. Lei, S. Matsuishi, H. Hosono and T. Kamiya, *J. Am. Chem. Soc.*, 2014, **136**, 14959–14965.
61 S. E. Harrison, *Phys. Rev.*, 1954, **93**, 52–62.
62 D. Ju, H. Xu, Z. Qiu, J. Guo, J. Zhang and B. Cao, *Sens. Actuators, B*, 2014, **200**, 288–296.